A 128-ch Area-Efficient Neurochemical-Sensing Front-End for FSCV Recordings of Dopamine

Kevin A. White, *Member, IEEE*, Mahdieh Darroudi, Jinwoo Park, and Brian N. Kim, *Senior Member, IEEE*

***Abstract*—Neurochemical recordings rely on electrochemical reactions of electroactive neurotransmitters such as dopamine, serotonin, and norepinephrine. This electrochemical technique allows for highly sensitive monitoring of neurotransmitters in the brain. Traditionally, single-channel carbon-fiber microelectrode (CFE) recordings have been considered the gold standard method. However, an alternative approach involves the use of a microelectrode array, which enables high spatiotemporal resolution imaging of electroactive neurotransmitters. To enable neurochemical imaging using a microelectrode array, the development of a high-density current-sensing microchip is necessary. Here, a neurochemical microchip is introduced, featuring a 128-channel current sensing front-end capable of supporting 128 parallel neurochemical measurements. The designed amplifier array employs a highly scalable resistive feedback transimpedance amplifier design. This design allows for a large neurochemical dynamic range of ±5 μA with a noise performance as low as 0.22 nA_{RMS}. The presented current sensing front end is validated by electrochemical detection of dopamine, by fast-scan cyclic voltammetry (FSCV) at 400 V/s, using an external carbon-fiber electrode in an electrochemical flow cell.**

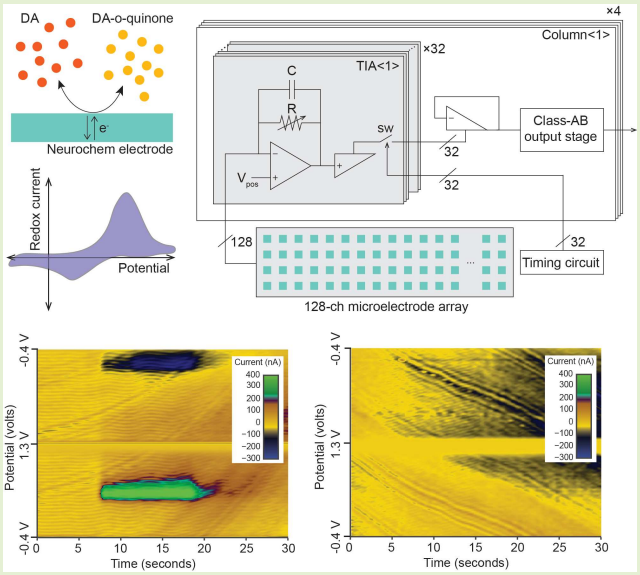

***Index Terms*—Current-sensing, dopamine, electrochemistry, fast-scan cyclic voltammetry (FSCV), microelectrode array, neural interface, neurochemical recordings, neurotransmitters.**

I. Introduction

HIGH spatiotemporal resolution imaging of dopamine in the brain is essential to study its complex interactions and functions in different regions and neural circuits. Dopamine (DA) is a key neurotransmitter that plays a crucial role in a wide range of neurological processes, including motivation, reward, and addiction. By imaging dopamine in real-time and with high spatial resolution, we can help elucidate the neurological function of neurochemicals in the central nervous system [2], [3], [4], [5], [6]. Moreover, high spatiotemporal resolution imaging of dopamine is critical for investigating dopamine-related disorders such as Parkinson's disease, schizophrenia, and Alzheimer's disease. Precise localization of dopamine release and uptake dynamics could aid in the identification of potential biomarkers or therapeutic targets for these disorders.

Electrochemical recordings of dopamine are widely used in neuroscience research as they provide real-time, highly sensitive measurements of dopamine release and uptake dynamics in the brain. These recordings are based on the electrochemical reactions of dopamine and other electroactive neurotransmitters at the surface of an electrode, which generates a current proportional to the amount of neurotransmitter present. Single-channel carbon-fiber microelectrode (CFE) recordings have been the gold standard for neurochemical recordings, but they are limited in their ability to capture spatial variations in neurotransmitter release. Current-sensing analog front ends are used as bioinstrumentation to apply a potential to an electrode to induce redox reactions while measuring the redox current (Fig. 1). Although a single CFE is commonly uti-

Manuscript received 25 October 2023; accepted 24 January 2024. Date of publication 5 February 2024; date of current version 14 March 2024. This work was supported by the National Science Foundation (NSF) under Grant 2133225 and Grant 2143140. The associate editor coordinating the review of this article and approving it for publication was Prof. Pai-Yen Chen. *(Corresponding author: Brian N. Kim.)*

Kevin A. White, Mahdieh Darroudi, and Brian N. Kim are with the Department of Bioengineering, The University of Texas at Dallas, Richardson, TX 75080 USA (e-mail: kevin.white@utdallas.edu; mahdieh.darroudi@utdallas.edu; bkim@utdallas.edu).

Jinwoo Park is with the Department of Biotechnical and Clinical Laboratory Sciences, The University at Buffalo, Buffalo, NY 14214 USA (e-mail: jinwoopa@buffalo.edu).

Digital Object Identifier 10.1109/JSEN.2024.3359892

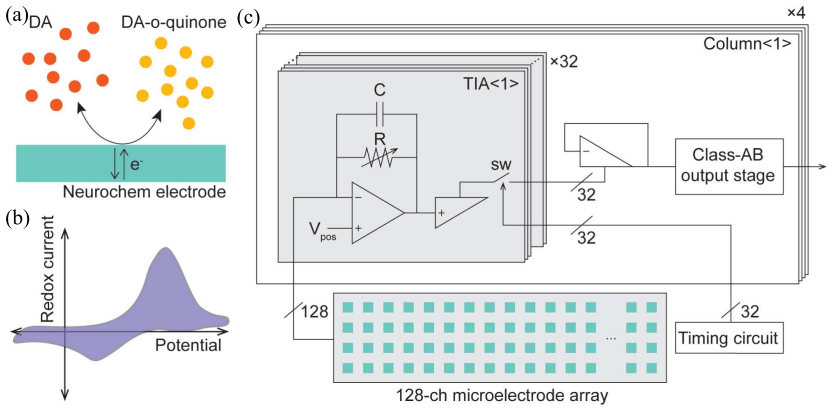

Fig. 1. Dopamine (DA) detection using 128-ch neurochemical front-end and FSCV. (a) Dopamine is detected by redox reactions at an electrode using FSCV, wherein molecules lose electrons (oxidation) or gain electrons (reduction). (b) FSCV recordings provide identification of a molecule, as well as the quantity of molecules, by the location and intensity of redox peaks versus the electrode potential. (c) Neurochemical sensing system incorporates a 128-ch neurochemical front-end for FSCV recordings using resistive-feedback TIA.

lized for in vivo monitoring of dopamine activity through fast-scan cyclic voltammetry (FSCV) [Fig. 1(b)] [2], [9], [10], [11], [12], [13], [14], a microelectrode array can offer a high spatiotemporal resolution by gathering neurochemical activity from a particular brain region to generate neurotransmitter mapping. To enable the operation and recording of a microelectrode array with a large number of electrodes (hundreds), a microchip containing an equal number of amplifiers is necessary to facilitate highly parallel electrochemical recordings [15], [16]. With the development of high-density microchips for processing and amplifying the small redox signals generated by these microelectrodes, electrochemical recordings of dopamine can provide a powerful tool for investigating the complex dynamics of dopamine signaling in the brain and its role in neurological diseases. Additionally, CMOS circuits and devices have been developed for high-density electrophysiological recordings [19], [20], [21], [22], and future multimodal CMOS bioelectronics may provide unique insight into brain functionality by providing simultaneous neurochemical and electrophysiological mapping of brain activity.

Typically, resistive feedback or integrating amplifier topologies are used to design analog front ends for electrochemical recordings. An integrating amplifier uses an operational amplifier (OPA) to regulate the electrode's potential and collects the electrode's current through a capacitor. The voltage change across the capacitor is then periodically read to monitor the current detected by the electrode. The main advantage of integrating amplifiers is their low noise characteristics [15], [23], [24], [25], [26], [27], [28], [29]; however, for large-dynamic range applications such as in vivo neurochemical recordings, the capacitor size can become too large, and integrating hundreds of amplifiers with a small and scalable silicon footprint can be challenging. For example, to achieve a $\pm 5\ \mu$A dynamic range with a 20 kHz sampling rate, the integration capacitor must be around 150 pF. A CMOS potentiostat using a 50-fF integration capacitor was only able to record between ± 1.5 nA [23]. Another CMOS potentiostat using a 50 to 150 fF integration capacitor also has a limited dynamic range of 60 nA [30]. Although it is possible to integrate a few 150 pF capacitors using CMOS technology, it is challenging to integrate 100 s of amplifiers. Current division or current subtraction can be used to decrease the required capacitance [1], [7], [8]; however, they come with a cost of power, area, or noise performance. An analog front-end with analog background subtraction was able to achieve high bandwidth (5 kHz) and low noise level (26.5 pA_{RMS}); however, the analog front-end size was relatively larger (0.256 mm^2) compared to other works that can achieve similar dynamic range [1]. Another subtraction-based circuit had a smaller footprint (0.06 mm^2), however, it suffered from a significant noise floor (10 pA/$\sqrt{}$Hz). Resistive feedback-based transimpedance amplifiers (TIA) can be suitable for large-dynamic range applications because the feedback resistors (around 1 MΩ and smaller) can be relatively smaller compared to equivalent capacitors (around 200 $\times$ 30 μm for 1 MΩ in a standard 0.35 μm process) [17].

In this article, we present a high-density neurochemical-sensing analog front-end microchip that integrates 128 resistive TIAs with multiplexers to support fully parallel 128-ch FSCV recordings of electrochemical activity [Fig. 1(c)]. The article is organized as follows. In Section II, the design of the neurochemical-sensing microchip and the circuit implementation are described. The characterization of gain, noise, and bandwidth performances are discussed in Section III. Section IV describes the carbon-fiber electrode fabrication and dopamine recordings using the neurochemical microchip, an external carbon fiber electrode, and an electrochemical flow cell. Finally, the conclusions and discussions are described in Section V.

II. Highly Scalable Neurochemical-Sensing Amplifiers

To design a large array of TIAs, it is critical to develop a TIA that occupies a small footprint. While both resistive and capacitive feedback are commonly used, we consider both options to minimize the design area.

A. Highly Scalable Transimpedance Amplifier Design

In a standard 0.35 μm process, a poly capacitor has a capacitance density of 0.90 fF/μm^2. Instead, an n-well resistor is 1000 Ω/square and a poly resistor is 50/square. Given that

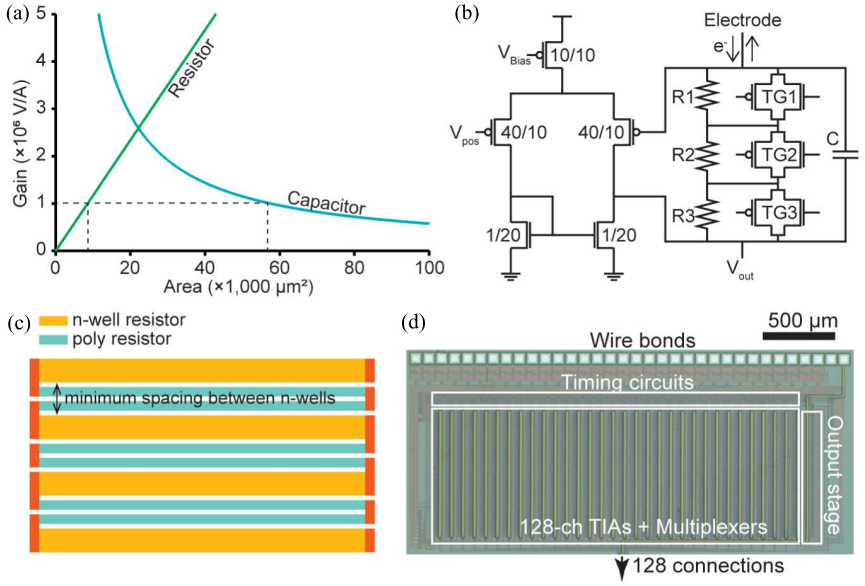

Fig. 2. Resistive feedback TIAs for 128-ch neurochemical sensing using FSCV. (a) Optimal transimpedance gain is in the range of 0.1–1 μA/V. To achieve this, a feedback resistor-based TIA can provide comparable gain to an integration capacitor-based TIA with lower area investment in layout. (b) Embedded transmission gate switches TG1–TG3 enable configurable TIA gain in tandem with the segmented feedback resistance. The feedback resistance directly determines the gain of the TIA and the gain on the scale of 100 kΩ–1 MΩ can be configured. The dimensions shown are W/L and are in μm. (c) To achieve maximum area efficiency when creating the layout, poly resistors are used in the spacing required between the n-well resistors for maximum resistance density. (d) Current sensing front-end has 128 parallel channels for neurochemical detection with the presented feedback resistor TIA arranged in a 4 × 32 array.

the minimum width of a n-well resistor is 3 μm (minimum square of 3 × 3 μm^2 according to the design rule), the resistance density can be calculated to be 110–120 Ω/μm^2. This translates to an achievable gain per unit area of 110–120 V/A/μm^2 [Fig. 2(a)]. Therefore, using resistive feedback, the gain increases linearly with the invested area.

In an integrating amplifier that uses capacitive feedback, the transimpedance gain is set by the integration time and capacitance:

$$\text{Gain [V/A]} = \frac{t_{\text{int}}}{C_{\text{int}}} \tag{1}$$

where C_{int} is the value of the integration capacitor and t_{int} is the integration duration. Assuming a sampling rate of 20 kS/s, the highest integration time that can be allocated is 50 μs. The gain determined by the poly capacitor is 6 × 10^{10} V·μm^2/A. When the targeted transimpedance gain is 1 × 10^6 V/A, the resistive feedback requires substantially less space (9000 μm^2) compared to that of capacitive feedback (60 000 μm^2) [Fig. 2(a)]. Based on the gain-area plot, the integration capacitor becomes more area-efficient than the resistor when the desired gain is beyond 2.6 × 10^6 V/A. For FSCV measurements coupled with microelectrodes, the targeted transimpedance gain is typically between 0.1 and 1 μA/V, corresponding to 100 kΩ–1 MΩ. Therefore, the resistive TIA is significantly more area-efficient.

Our TIA design is based on resistive feedback in which the incoming redox current is multiplied by the resistance and directly changes the amplifier's output voltage [Fig. 2(b)]. The feedback resistance is divided into three resistors to enable programmable transimpedance gain. Each segmented resistor is linked to a parallel transmission gate (TG1–3), which allows for adjustable transimpedance gain. The three transmission gate switches can be configured to produce 2^3 different gain settings. Because n-well resistors achieve the highest resistance density compared to other types of resistors present in the CMOS technology, n-well resistors are the preferred option for the highly scalable TIA design. However, the design rule sets a minimum spacing (typically equivalent to the minimum width of an n-well resistor) between n-wells with different potentials which adds a large overhead in integrating multiple segments of n-well resistors in series. This rule is to avoid significant current flow between n-wells. This drops the achievable gain per unit area to 55–60 V/A/μm^2. To maximize the resistance density, poly resistors can be added within the spacings [Fig. 2(c)]. Although the resistance per square for poly resistors is far smaller compared to that of n-well resistors, because the minimum width is smaller (below 1 μm^2), the resistance density is 60 Ω/μm^2, nearly half of that of n-well resistors. The three feedback resistors are made up of a combination of n-well resistors and poly resistors [as shown in Fig. 2(c)]. This configuration provides the highest resistor density per area without violating layout design rules (85–90 V/A/μm^2), which will still produce a higher gain compared to a capacitive design.

The transistor dimensions are selected to optimize the area efficiency while preserving gain, bandwidth, power efficiency, and uniformity based on Monte Carlo simulation [Fig. 2(b)]. The feedback capacitor restricts the bandwidth to a range of 10–100 kHz. The oxidation/reduction current flows through the feedback resistor, creating the transimpedance gain at the OPA's output. Each TIA occupies 220 × 80 μm (0.0176 mm^2) of space. A total of 128 TIAs occupies only 2.25 mm^2 silicon space [Fig. 2(b)].

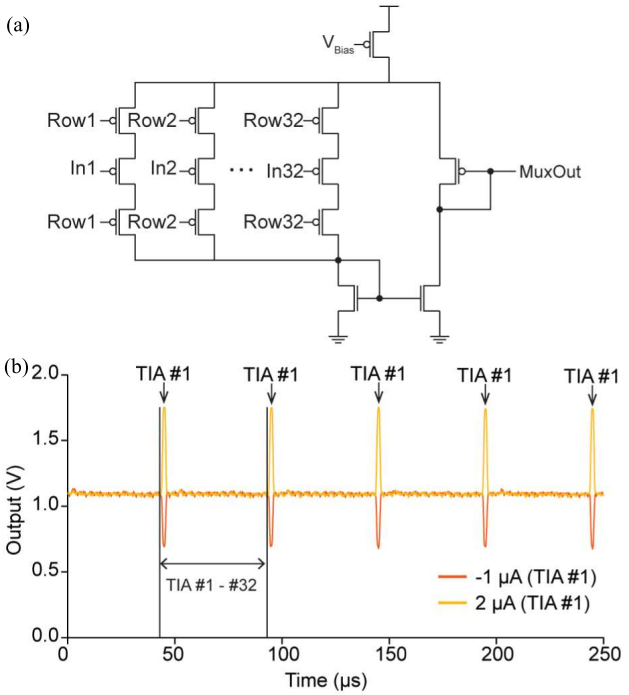

Fig. 3. To reduce the number of outputs, the amplifiers' outputs are combined in groups of 32 using time-division multiplexing. (a) Multiplexer is a half-shared structure. The non-inverting side is embedded in each amplifier and the inverting side is shared as a multiplexer output. (b) To demonstrate the time-division multiplexing output, the output of TIA #1, which is connected to In1 of the multiplexer, is measured. This TIA has an input current of either -1 or 2 μA while all other TIAs have 0 input current. At a 20 kHz sampling rate, the output of TIA #1 will be seen every 50 μs.

B. Time-Division Multiplexing

To reduce the number of outputs, the amplifiers' outputs are combined in groups of 32 as columns using time-division multiplexing. The system comprises four columns with a total of 128 fully parallel TIAs. The time-division multiplexing is based on a half-shared amplifier that connects individual TIA's outputs to the output stages using switches [15], [25], [27]. Each TIA contains an embedded non-inverting OPA (three transistors), which links to an inverting OPA in each column via a switch [Fig. 3(a)]. When Row1 is low (active low), the other row switches (Row2–Row32) are high so that only In1 is the unity gain input to the multiplexer's output, MuxOut. In a 50-μs interval, all 32 inputs (In1–In32) are multiplexed to MuxOut by staggering the switches (Row1–Row32). The output in Fig. 3(b) shows the multiplexed output where a TIA connected to In1 (TIA #1) has an input current of -1 or 2 μA. For this test, the rest of the TIAs have zero input current and therefore result in a flat output.

C. System Integration

The system consists of 128 TIAs, multiplexers, timing circuits, and output stages [Fig. 1(c)].As the outputs from this system are sampled using external analog-to-digital converters (ADC), class-AB output stages are designed within the system to drive large capacitive loads originating from the ADC's input capacitance and the line capacitance. The timing circuit produces all the sub-clocks required to run this multiplexing scheme. The amplifier array is fabricated using a standard 2-poly 4-metal 0.35-μm process (Fig. 2). This process is chosen because of its wide voltage range. The amplifier array, timing circuit, output stage, and wire bonds occupy 3.05 $\times$ 1.37 mm.

In order to connect external electrodes to the amplifier array, such as a single CFE as discussed in Section IV, post-CMOS processing is performed. In brief, negative resist NR9-1500PY is used to create a sacrificial lift-off layer to pattern the bonding pads for external electrode connection. With the patterned sacrificial layer created, 20 nm of titanium and then 200 nm of platinum are deposited by sputtering. The negative resist is then removed by rinsing the chip with acetone. Then the chip is bonded to a custom PCB that allows the bonding pads created by post-CMOS processing to be connected to either external electrodes or an external microelectrode array.

III. Performance and Characteristics

Transimpedance gain, bandwidth, noise, and crosstalk of the TIA are evaluated in this section. For all tests, USB-6363 (National Instruments) is used for analog data acquisition. Current signals are generated using either USB-6363 DAQ for alternating current or a source/measure unit (B2901A, Keysight) for constant current. For noise measurements, the chip is powered using battery-powered voltage regulators to minimize the contribution of line frequency. For all data acquisitions, a custom-designed LabVIEW program is used. In this program, the clock source that governs the data sampling is synchronized with that of digital-to-analog converters (DACs) so that the artificial signals being injected into the amplifier have a sharply defined frequency component. This is beneficial in analyzing the frequency response of the amplifiers.

A. Measured Transimpedance Gain

To determine the gain of the current sensing front-end, an external current is introduced into the amplifier and the resulting change in output voltage is recorded [Fig. 4(a)]. Across the dynamic range shown, the amplifier exhibits a highly linear response in four gain settings, with an R^2 value of 0.999 for all gain settings. The dynamic range can vary from as high as ± 5 μA (Gain 4) to as low as ± 650 nA (Gain 1). Furthermore, the uniformity of the transimpedance gain across the array is evaluated. Any mismatch in the dimensions of devices in each TIA can contribute to non-uniformity in performance characteristics. The array demonstrates a consistent gain across the 128 amplifiers in the array [as Fig. 4(b)], with measured gains of 1.16 ± 0.04 MΩ, 618.93 ± 13.3 kΩ, 314 ± 9.63 kΩ, and 127 ± 2.17 kΩ (mean $\pm$ SD) for Gain 1, Gain 2, Gain 3, and Gain 4, respectively. The transimpedance gains plotted in histograms show Gaussian distributions for each gain setting [Fig. 4(b)]. Because this deviation is systematic, gains of each amplifier can be measured during a calibration step and subsequently applied individually to each amplifier's recordings to accurately represent the measured current.

B. Bandwidth, Noise, and Crosstalk

To test the bandwidth of the amplifier, sinusoidal currents (100 Hz–300 kHz) are injected into the amplifier while

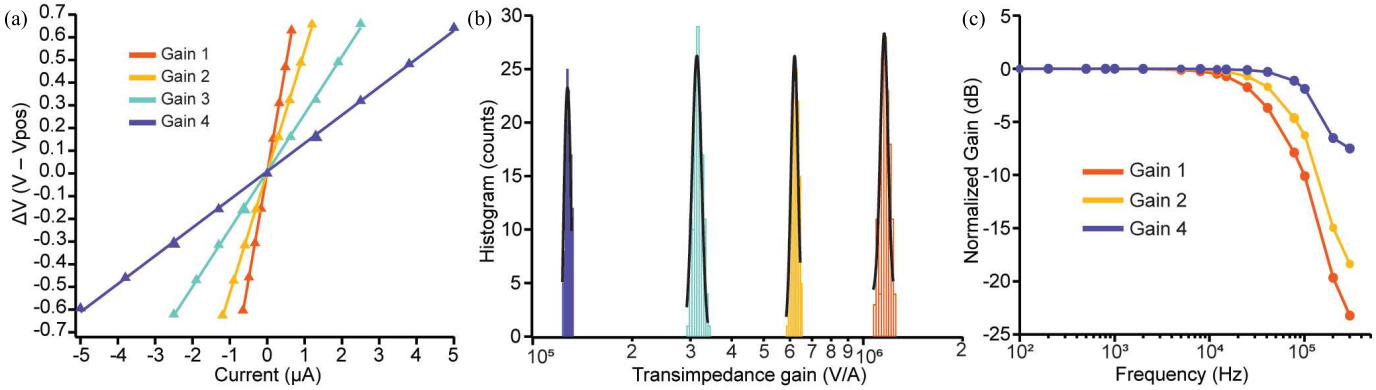

Fig. 4. Measured transimpedance gain across the entire 128-amplifier array. (a) Gain calibration shows highly linear responses across the dynamic range with an R^2 of 0.999 for all gain settings. (b) 128-ch current sensing front-end exhibits a relatively consistent gain across the array with measured gains of 1.16 ± 0.04 MΩ, 618.93 ± 13.31 kΩ, 314.00 ± 9.63 kΩ, and 127.27 ± 2.17 kΩ (mean ± SD) for Gain 1, Gain 2, Gain 3, and Gain 4, respectively. (c) Measured bandwidth of the TIA for Gain 1, Gain 2, and Gain 4 (measured cutoff frequencies of 40, 53, and 122 kHz, respectively).

monitoring the response at the output [Fig. 4(c)]. For the three gain settings tested, the cutoff frequencies are 40, 53, and 122 kHz for Gain 1, Gain 2, and Gain 4, respectively. Because the cutoff is determined by $R_f C_f$, the lowest gain setting (Gain 4) exhibits the widest bandwidth. Because in most cases, a constant bandwidth is desirable across gain settings, a second stage behaving as a low-pass filter can be placed to eliminate the variability. However, in this application, to minimize the footprint of each TIA, an additional low-pass filter is not used.

The noise characteristics are measured as functions of gain setting and biasing level. The output of the amplifier is sampled at 640 kS/s (Fig. 5). The noise level of the amplifier is 0.22, 0.42, and 1.99 nA_{RMS} for Gain 1, Gain 2, and Gain 4, respectively. For three different bias levels between 1.1 μA to 20.1 μA (Gain 1), no appreciable difference is observable in the noise of the amplifier [Fig. 5(b)].

Crosstalk can often hinder the ability to provide independent high-density recordings. To verify the isolation between amplifiers in an array, it is important to examine crosstalk. Crosstalk is evaluated by introducing a large sinusoidal current (with a peak-to-peak amplitude of 0.8 μA and a frequency of 625 Hz) that covers almost the entire input dynamic range into one amplifier and observing the spectral response of neighboring amplifiers (as shown in Fig. 6). The highest gain setting (Gain 1) is used for this experiment to test the worst-case scenario. In the time domain, the crosstalk between the physically neighboring amplifiers is invisible [as shown in Fig. 6(a)]. In the spectral responses, the crosstalk is measured at adjacent amplifiers and found to be −82.5, −83.2, and −89.7 dBc [as depicted in Fig. 6(b)], showing nearly complete isolation between amplifiers.

IV. Dopamine Recordings Using Carbon-Fiber Electrode

To validate the neurochemical-sensing front-end for dopamine measurement, one of the amplifier's inputs is connected to a CFE. Using a flow cell setup, dopamine is introduced to the electrode while FSCV recordings are performed.

A. Carbon-Fiber Electrode Fabrication

The CFE fabrication process is based on a previously reported method [12], [14]. In brief, a 7-μm carbon fiber is threaded in through a glass capillary using a vacuum. Then, the glass capillary loaded with carbon fiber is pulled using a micropipette puller (P-87, Sutter Instrument) which creates two glass pipettes with carbon fiber. The carbon fiber extending from the tip of the glass pipette is initially trimmed using a surgical scissor to a few millimeters in length. Subsequently, the glass pipette with carbon fiber is placed under a microscope and the carbon fiber is additionally trimmed using a surgical blade to 140 μm in length. The resulting carbon-fiber electrode has a sensing area of 3100 μm^2. The carbon fiber is connected to a 22 AWG wire using silicon epoxy on the opposite side of the glass capillary.

B. Flow Cell Experiment

In order to introduce dopamine to the electrode with precision, a flow cell is typically used. For this experiment, an In vitro/FSCV microelectrode flow cell is used (NEC-FLOW-1, Pine Research). This flow cell is based on gravity feed. The fluid sample is loaded from below a flow channel (electrode channel) in which the carbon-fiber electrode is directly inserted. An Ag|AgCl reference electrode is used which is set to 1.55 V. This is to provide negative potential across the electrode-electrolyte interface without operating the CMOS chip at negative potentials. By default, phosphate-buffered saline (PBS) flows through the electrode channel with a flow rate of 1 mL/min. Dopamine solution can be added to this flow using an HPLC valve switch. This injection is governed by a syringe pump which controls the injection time, volume, and flow rate of dopamine solution (0.5–10 μM).

C. FSCV Recordings of Dopamine

All TIAs have a shared V_{pos} connection. The voltage ramp for FSCV is applied to the V_{pos} node at each TIA and sweeps from 1.15 to 2.85 V at a scan rate of 400 V/s. Against the Ag|AgCl reference electrode, the ramp range is between

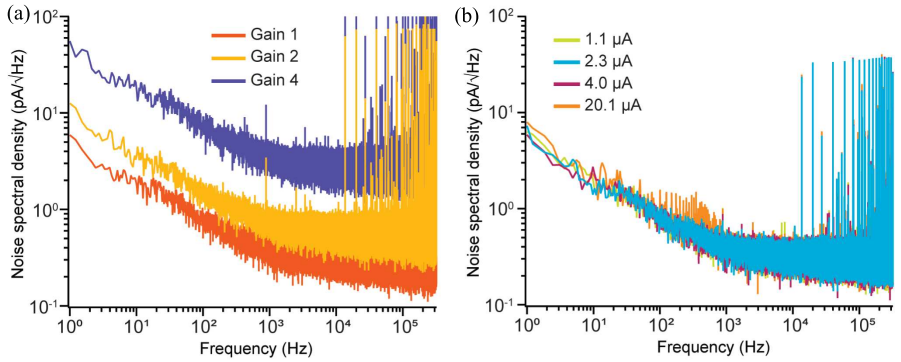

Fig. 5. Noise characteristics in various TIA gain settings and biasing current. (a) Noise level of the amplifier is 0.22 nA_{RMS}, 0.42 pA_{RMS}, and 1.99 nA_{RMS} for Gain 1 (highest transimpedance gain), Gain 2, and Gain 4 (lowest transimpedance gain) respectively. (b) For bias levels between 1.1 and 20.1 μA at setting Gain 1, the noise density is consistent.

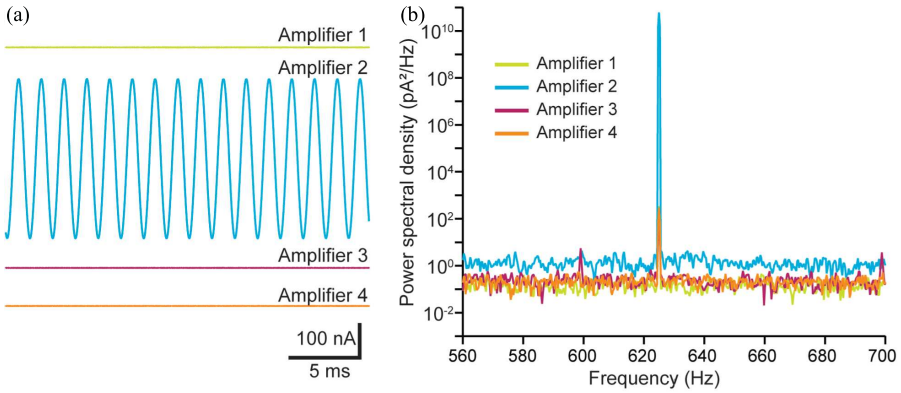

Fig. 6. Crosstalk experiment with a sinusoidal current is injected into Amplifier 2. (a) In the time domain, no crosstalk is observable. (b) Spectral analysis shows a small level of crosstalk in the adjacent amplifiers (−82.5, −83.2, and −89.7 dBc).

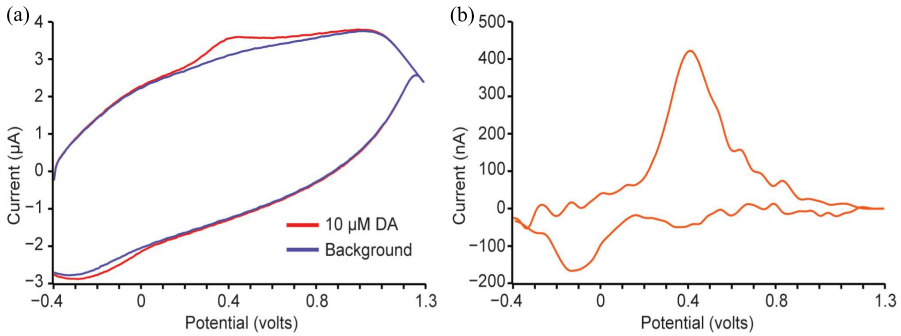

Fig. 7. Fast-scan cyclic voltammogram using the neurochemical chip and an external CFE. (a) In the background measurement, the CFE measures a current signal in PBS without dopamine (DA). This measured current is mostly from the double-layer capacitance of the electrode-electrolyte interface. The measurement is repeated with 10-μM DA in PBS. Redox peaks are visible near 0.4 and −0.2 V. (b) 10-μM DA measurement is subtracted using the background measurement to show the redox reactions of DA.

−0.4 and 1.3 V (E versus Ag|AgCl). The FSCV voltage ramp is repeated every 100 ms with an arresting potential of −0.4 V.

During the recording session, the PBS buffer is used as a default solution with a continuous flow rate of 1 mL/min. After 5–7 s of initial recording, DA solution is injected into the flow stream. For background subtraction, the initial 5-s FSCV recordings are averaged to create the background voltammogram.

For the 10-μM DA recording, the voltammogram taken after the DA injection shows distinct redox peaks compared to the background current [Fig. 7(a)]. Using the background subtraction, redox peaks are visible at 400 and −100 mV [Fig. 7(b)], consistent with previous CFE-based DA FSCV recordings [12], [31], [32]. The presented CFE-based DA recordings validate the neurochemical-sensing front end for dopamine detection. The recorded cyclic voltammograms can be plotted in a 2-D image to visualize the oxidation and reduction of DA in time [Fig. 8(a) and (b)]. The presence of dopamine can be seen between 7 and 20 s with strong oxidation and reduction currents [Fig. 8(a)]. In a control experiment in which PBS is injected without DA, redox currents are not detected as expected [Fig. 8(b)]. The oxidation

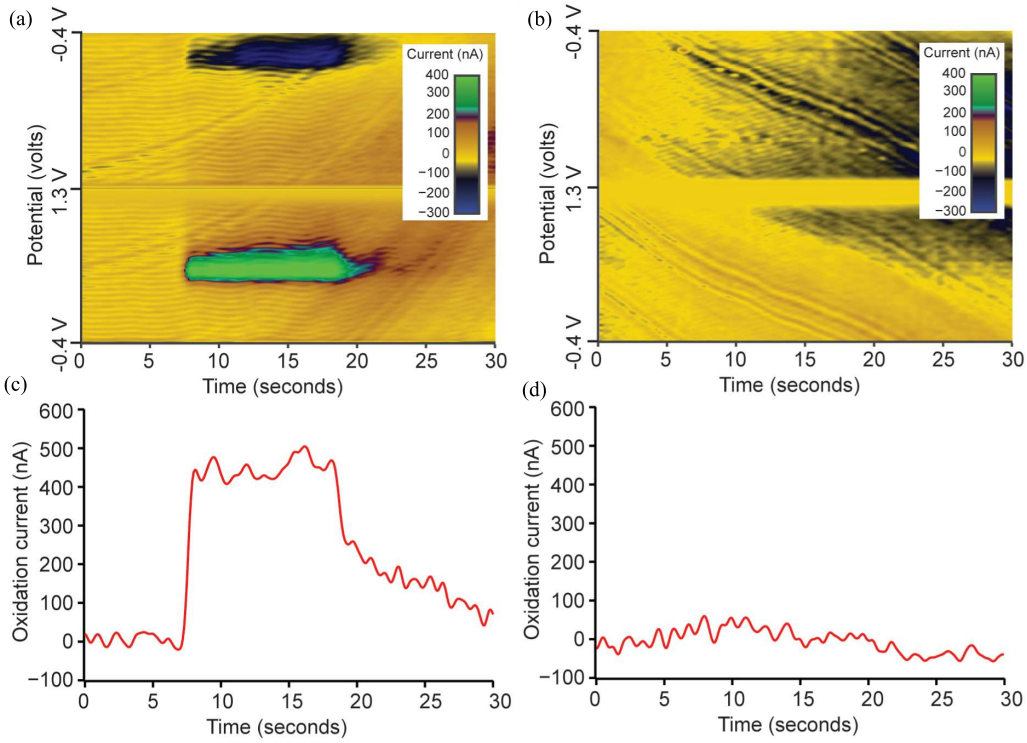

Fig. 8. Two-dimensional cyclic voltammogram using the neurochemical microchip and an external CFE. (a) and (b) CFE is mounted on a flow cell where dopamine (DA) is introduced between 5 and 7 s into the recording. For the control experiment, instead of DA, PBS is introduced. (c) and (d) Oxidation peaks of all the cycles are extracted for both DA measurement and control experiment.

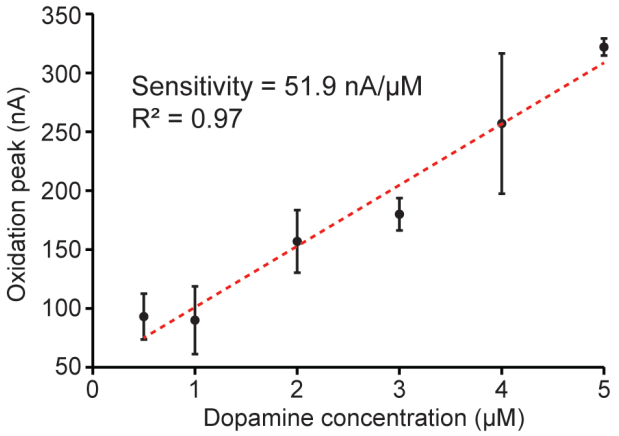

Fig. 9. DA sensitivity of CFE and neurochemical-sensing front end. The error bar is in the standard error of means.

peaks from individual cycles can be extracted to visualize the time-domain DA measurement. By extracting the oxidation currents at 400 mV, the transient response of DA shows a rapid increase in the oxidation of DA at 7 s, which continues for 13 s before tapering down [Fig. 8(c)]. No visible response is recorded in the control experiment [Fig. 8(d)], confirming that the current measured in the DA experiment is from the DA oxidation. Small ripplings in both 2-D voltammograms are originating from 60 Hz noise which is likely due to the largely unshielded connection between the CFE and the amplifier chip. In practice, the amplifier chip will be used as a headstage amplifier chip that is in close proximity to the neural probe (<10 cm), and therefore, the 60 Hz noise will be substantially smaller.

In general, CFE should have a linear response to DA concentrations below 5 μM [31], [33], [34]. The flow cell experiment is repeated for various DA concentrations between 0.5 and 5 μM. The DA sensitivity of the CFE and the neurochemical-sensing front end is tested by plotting the oxidation currents for each DA concentration (Fig. 9). Each experiment is repeated three times. The sensitivity is 51.9 nA/μM which is consistent with previous reports of DA detection using CFE [12].

V. Conclusion and Discussion

This article introduces a high-density neurochemical microchip. In low-noise applications, an integration capacitor-based TIA is a common approach. However, for FSCV applications, a wide dynamic range is required, which necessitates a substantial area investment for these integration capacitors. This can be problematic when designing a large array of amplifiers. To address this, we investigated using n-well and poly resistors as feedback resistors to develop our scalable TIAs. The resistive TIAs we present have a small footprint of 220 × 80 μm and exhibit low-noise characteristics (0.22 nA_{RMS}) that are suitable for in vivo neurochemical applications. The noise floor for the highest gain setting (BW = 40 kHz) is 1.1 pA/$\sqrt{\text{Hz}}$. We achieved a wide dynamic range of $\pm$5 μA, which can be expanded further by opting for a smaller resistance value, albeit at the expense of noise characteristics and resolution.

TABLE I
COMPARISON TO STATE-OF-THE-ART CURRENT SENSING FRONT-ENDS

	Ying TBIOCAS '22 [1]	Zamani MWSCAS '20 [7]	Lu TBIOCAS '21 [8]	Valente EMBC '16 [17]	Nasri TBIOCAS '17 [18, 19]	**This Work**
AFE Type	Current conveyor	Current input -ΔΣ	I-to-F converter	Resistive TIA	Dual-slope integrating ADC	**Resistive TIA**
Technology Node (nm)	180	180	180	180	65	**350**
Channel Count	1	1	1	3	4	**128**
Channel Area (mm^2)	0.256	0.06	-	0.21	0.075	**.0176**
Total Die Area (mm^2)	-	-	3.17	9.95	-	**4.18**
On-chip ADC	Yes	Yes	Yes	Yes	Yes	**No**
Supply Voltage (V)	3.3	2.5	1.2 - 1.5	1.8	1.8	**4**
Power/Ch (µW)	3.7	14.2	19	954	3.1	**4.4**
Noise (nA_{RMS})	0.027	0.71	25	0.292	0.02	**0.22**
Bandwidth (kHz)	5	5	50	100	1	**40-122**
Noise Density (pA/√Hz)	0.38	10	111	0.92	0.63	**1.1**
Input Range (µA)	0.375	± 1.5	-7 - +10	10	± 2.56	**± 5**

Compared to previously published works (Table I), our amplifier design achieves one of the lowest noise levels and smallest footprints. However, our approach uses off-chip ADCs for digitization which is beneficial in creating low power and small footprint circuits. Our future goal is to assess the amplifier's performance in FSCV applications by connecting it to a microelectrode array. This would enable high spatiotemporal resolution in vivo imaging of electroactive neurotransmitters in the brain, a feat not yet accomplished.

One of the key challenges in developing high-spatial recordings of neurochemicals is the development of robust microelectrode arrays that have a high level of specificity to faradaic current and stability without significant deterioration over time. While various materials have been tested for this purpose [35], [36], [37], [38], [39], carbon-based electrodes appear to be an appropriate candidate [39], [40], [41] for detecting electroactive neurotransmitters such as dopamine, epinephrine, norepinephrine, and serotonin. Additionally, electrode surface modifications are also being explored to enable the detection of neurotransmitters that are not electroactive, such as acetylcholine, choline, and L-glutamate [42], [43]. Our future work is aimed toward developing an on-chip microfabricated carbon-based electrode array in conjunction with this neurochemical chip to achieve high spatiotemporal resolution imaging of neurochemicals in vivo. The on-chip integration approach will bypass the bottleneck in scaling the number of electrodes.

ACKNOWLEDGMENT

The authors would like to thank the Advanced Microfabrication Facility (AMPAC) University of Central Florida staff for their support. They also thank the University of Florida Research Service Centers for their support in microfabrication.

REFERENCES

[1] D. Ying, J. Rosenberg, N. K. Singh, and D. A. Hall, "A 26.5 pArms neurotransmitter front-end with class-AB background subtraction," *IEEE Trans. Biomed. Circuits Syst.*, vol. 16, no. 4, pp. 692–702, Aug. 2022, doi: 10.1109/TBCAS.2022.3194809.

[2] M. L. A. V. Heien, M. A. Johnson, and R. M. Wightman, "Resolving neurotransmitters detected by fast-scan cyclic voltammetry," *Anal. Chem.*, vol. 76, no. 19, pp. 5697–5704, Oct. 2004, doi: 10.1021/ac0491509.

[3] M. K. Zachek, P. Takmakov, J. Park, R. M. Wightman, and G. S. McCarty, "Simultaneous monitoring of dopamine concentration at spatially different brain locations in vivo," *Biosensors Bioelectron.*, vol. 25, no. 5, pp. 1179–1185, Jan. 2010, doi: 10.1016/j.bios.2009.10.008.

[4] J. Park, K. T. Wakabayashi, C. Szalkowski, and R. V. Bhimani, "Heterogeneous extracellular dopamine regulation in the subregions of the olfactory tubercle," *J. Neurochem.*, vol. 142, no. 3, pp. 365–377, Aug. 2017, doi: 10.1111/jnc.14069.

[5] J. Park, R. Bhimani, K. Wakabayashi, and C. Bass, "In vivo electroanalytical measurements of norepinephrine in the brain: Current status and remaining challenges," *ECS Meeting Abstr.*, no. 55, p. 2305, Sep. 2017, doi: 10.1149/ma2017-02/55/2305.

[6] R. V. Bhimani, R. Yates, C. E. Bass, and J. Park, "Distinct limbic dopamine regulation across olfactory-tubercle subregions through integration of in vivo fast-scan cyclic voltammetry and optogenetics," *J. Neurochem.*, vol. 161, no. 1, pp. 53–68, Apr. 2022, doi: 10.1111/jnc.15577.

[7] H. Zamani, S.-A. Chan, C. Smith, and P. Mohseni, "A neurochemical recording microsystem with analog background current subtraction and 400V/s FSCV sensing using a 1st-order ΔΣM," in *Proc. IEEE 63rd Int. Midwest Symp. Circuits Syst. (MWSCAS)*, Aug. 2020, pp. 517–520, doi: 10.1109/MWSCAS48704.2020.9184687.

[8] S.-Y. Lu and Y.-T. Liao, "A 19 μW, 50 kS/s, 0.008-400V/s cyclic voltammetry readout interface with a current feedback loop and on-chip pattern generation," *IEEE Trans. Biomed. Circuits Syst.*, vol. 15, no. 2, pp. 190–198, Apr. 2021, doi: 10.1109/TBCAS.2021.3062377.

[9] R. M. Wightman, "Voltammetry with microscopic electrodes in new domains," *Science*, vol. 240, no. 4851, pp. 415–420, Apr. 1988, doi: 10.1126/science.240.4851.415.

[10] R. M. Wightman et al., "Temporally resolved catecholamine spikes correspond to single vesicle release from individual chromaffin cells," *Proc. Nat. Acad. Sci. USA*, vol. 88, no. 23, pp. 10754–10758, Dec. 1991.

[11] K. T. Kawagoe, J. B. Zimmerman, and R. M. Wightman, "Principles of voltammetry and microelectrode surface states," *J. Neurosci. Methods*, vol. 48, no. 3, pp. 225–240, Jul. 1993, doi: 10.1016/0165-0270(93)90094-8.

[12] D. L. Robinson, B. J. Venton, M. L. A. V. Heien, and R. M. Wightman, "Detecting subsecond dopamine release with fast-scan cyclic voltammetry in vivo," *Clin. Chem.*, vol. 49, no. 10, pp. 1763–1773, Oct. 2003, doi: 10.1373/49.10.1763.

[13] D. L. Robinson, A. Hermans, A. T. Seipel, and R. M. Wightman, "Monitoring rapid chemical communication in the brain," *Chem. Rev.*, vol. 108, no. 7, pp. 2554–2584, Jul. 2008.

[14] N. T. Rodeberg, S. G. Sandberg, J. A. Johnson, P. E. M. Phillips, and R. M. Wightman, "Hitchhiker's guide to voltammetry: Acute and chronic electrodes for in vivo fast-scan cyclic voltammetry," *ACS Chem. Neurosci.*, vol. 8, no. 2, pp. 221–234, 2017, doi: 10.1021/acschemneuro.6b00393.

[15] B. N. Kim, A. D. Herbst, S. J. Kim, B. A. Minch, and M. Lindau, "Parallel recording of neurotransmitters release from chromaffin cells using a 10 × 10 CMOS IC potentiostat array with on-chip working electrodes," *Biosensors Bioelectron.*, vol. 41, pp. 736–744, Mar. 2013, doi: 10.1016/j.bios.2012.09.058.

[16] J. Rothe, O. Frey, A. Stettler, Y. Chen, and A. Hierlemann, "Fully integrated CMOS microsystem for electrochemical measurements on 32 × 32 working electrodes at 90 frames per second," *Anal. Chem.*, vol. 86, no. 13, pp. 6425–6432, Jul. 2014, doi: 10.1021/ac500862v.

[17] V. Valente, D. Jiang, and A. Demosthenous, "Dual-mode CMOS analog front-end (AFE) for electrical impedance spectroscopy (EIS) systems," in *Proc. 38th Annu. Int. Conf. IEEE Eng. Med. Biol. Soc. (EMBC)*, Aug. 2016, pp. 1914–1917, doi: 10.1109/EMBC.2016.7591096.

[18] B. Nasri et al., "Hybrid CMOS-graphene sensor array for subsecond dopamine detection," *IEEE Trans. Biomed. Circuits Syst.*, vol. 11, no. 6, pp. 1192–1203, Dec. 2017, doi: 10.1109/TBCAS.2017.2778048.

[19] J. Abbott et al., "A nanoelectrode array for obtaining intracellular recordings from thousands of connected neurons," *Nature Biomed. Eng.*, vol. 4, no. 2, pp. 232–241, Sep. 2019, doi: 10.1038/s41551-019-0455-7.

[20] U. Frey et al., "Switch-matrix-based high-density microelectrode array in CMOS technology," *IEEE J. Solid-State Circuits*, vol. 45, no. 2, pp. 467–482, Feb. 2010, doi: 10.1109/JSSC.2009.2035196.

[21] D. Tsai, D. Sawyer, A. Bradd, R. Yuste, and K. L. Shepard, "A very large-scale microelectrode array for cellular-resolution electrophysiology," *Nature Commun.*, vol. 8, no. 1, p. 1802, Nov. 2017, doi: 10.1038/s41467-017-02009-x.

[22] B. Eversmann et al., "A 128 × 128 CMOS biosensor array for extracellular recording of neural activity," *IEEE J. Solid-State Circuits*, vol. 38, no. 12, pp. 2306–2317, Dec. 2003, doi: 10.1109/JSSC.2003.819174.

[23] C. I. Dorta-Quiñones et al., "A bidirectional-current CMOS potentiostat for fast-scan cyclic voltammetry detector arrays," *IEEE Trans. Biomed. Circuits Syst.*, vol. 12, no. 4, pp. 894–903, Aug. 2018, doi: 10.1109/TBCAS.2018.2828828.

[24] K. A. White and B. N. Kim, "Quantifying neurotransmitter secretion at single-vesicle resolution using high-density complementary metal-oxide-semiconductor electrode array," *Nature Commun.*, vol. 12, no. 1, pp. 1–8, Jan. 2021, doi: 10.1038/s41467-020-20267-0.

[25] K. A. White et al., "Single-cell recording of vesicle release from human neuroblastoma cells using 1024-ch monolithic CMOS bioelectronics," *IEEE Trans. Biomed. Circuits Syst.*, vol. 12, no. 6, pp. 1345–1355, Dec. 2018, doi: 10.1109/TBCAS.2018.2861220.

[26] K. A. White, G. Mulberry, and B. N. Kim, "Rapid 1024-pixel electrochemical imaging at 10,000 frames per second using monolithic CMOS sensor and multifunctional data acquisition system," *IEEE Sensors J.*, vol. 18, no. 13, pp. 5507–5514, Jul. 2018, doi: 10.1109/JSEN.2018.2835829.

[27] G. Mulberry, K. A. White, and B. N. Kim, "Analysis of simple half-shared transimpedance amplifier for picoampere biosensor measurements," *IEEE Trans. Biomed. Circuits Syst.*, vol. 13, no. 2, pp. 387–395, Apr. 2019, doi: 10.1109/TBCAS.2019.2897287.

[28] G. Mulberry, K. White, M. Crocker, and B. Kim, "A 512-ch dual-mode microchip for simultaneous measurements of electrophysiological and neurochemical activities," *Biosensors*, vol. 13, no. 5, p. 502, Apr. 2023. [Online]. Available: https://www.mdpi.com/2079-6374/13/5/502

[29] K. A. White, G. Mulberry, and B. N. Kim, "Parallel 1024-ch cyclic voltammetry on monolithic CMOS electrochemical detector array," *IEEE Sensors J.*, vol. 20, no. 8, pp. 4395–4402, Apr. 2020, doi: 10.1109/JSEN.2019.2961809.

[30] S. Kumashi et al., "A CMOS multi-modal electrochemical and impedance cellular sensing array for massively paralleled exoelectrogen screening," *IEEE Trans. Biomed. Circuits Syst.*, vol. 15, no. 2, pp. 221–234, Apr. 2021, doi: 10.1109/TBCAS.2021.3068710.

[31] B. J. Venton and Q. Cao, "Fundamentals of fast-scan cyclic voltammetry for dopamine detection," *Analyst*, vol. 145, no. 4, pp. 1158–1168, 2020, doi: 10.1039/c9an01586h.

[32] Y.-M. Shon et al., "Comonitoring of adenosine and dopamine using the wireless instantaneous neurotransmitter concentration system: Proof of principle: Laboratory investigation," *J. Neurosurgery*, vol. 112, no. 3, pp. 539–548, Mar. 2010, doi: 10.3171/2009.7.jns09787.

[33] E. S. Ramsson, "A pipette-based calibration system for fast-scan cyclic voltammetry with fast response times," *BioTechniques*, vol. 61, no. 5, pp. 269–271, Nov. 2016, doi: 10.2144/000114476.

[34] E. Sinkala, J. E. McCutcheon, M. J. Schuck, E. Schmidt, M. F. Roitman, and D. T. Eddington, "Electrode calibration with a microfluidic flow cell for fast-scan cyclic voltammetry," *Lab Chip*, vol. 12, no. 13, p. 2403, 2012, doi: 10.1039/c2lc40168a.

[35] K. Berberian, K. Kisler, Q. Fang, and M. Lindau, "Improved surface-patterned platinum microelectrodes for the study of exocytotic events," *Anal. Chem.*, vol. 81, no. 21, pp. 8734–8740, Nov. 2009, doi: 10.1021/ac900674g.

[36] K. Kisler et al., "Transparent electrode materials for simultaneous amperometric detection of exocytosis and fluorescence microscopy," *J. Biomaterials Nanobiotechnol.*, vol. 3, no. 2, pp. 243–253, 2012, doi: 10.4236/jbnb.2012.322030.

[37] S. Y. Yang et al., "Detection of transmitter release from single living cells using conducting polymer microelectrodes," *Adv. Mater.*, vol. 23, no. 24, pp. H184–H188, Jun. 2011, doi: 10.1002/adma.201100035.

[38] E. Castagnola et al., "Flexible glassy carbon multielectrode array for in vivo multisite detection of tonic and phasic dopamine concentrations," *Biosensors*, vol. 12, no. 7, p. 540, Jul. 2022, doi: 10.3390/bios12070540.

[39] H. Xu et al., "Selective recognition of 5-hydroxytryptamine and dopamine on a multi-walled carbon nanotube-chitosan hybrid film-modified microelectrode array," *Sensors*, vol. 15, no. 1, pp. 1008–1021, Jan. 2015. [Online]. Available: https://www.mdpi.com/1424-8220/15/1/1008

[40] J. Park, Y. Show, V. Quaiserova, J. J. Galligan, G. D. Fink, and G. M. Swain, "Diamond microelectrodes for use in biological environments," *J. Electroanal. Chem.*, vol. 583, no. 1, pp. 56–68, Sep. 2005, doi: 10.1016/j.jelechem.2005.04.032.

[41] J. Park, V. Quaiserová-Mocko, K. Pecková, J. J. Galligan, G. D. Fink, and G. M. Swain, "Fabrication, characterization, and application of a diamond microelectrode for electrochemical measurement of norepinephrine release from the sympathetic nervous system," *Diamond Rel. Mater.*, vol. 15, nos. 4–8, pp. 761–772, Apr. 2006, doi: 10.1016/j.diamond.2005.11.008.

[42] K. M. Mitchell, "Acetylcholine and choline amperometric enzyme sensors characterized in vitro and in vivo," *Anal. Chem.*, vol. 76, no. 4, pp. 1098–1106, Feb. 2004, doi: 10.1021/ac034757v.

[43] W. Wei et al., "An implantable microelectrode array for simultaneous L-glutamate and electrophysiological recordings in vivo," *Microsystems Nanoengineering*, vol. 1, no. 1, pp. 1–6, May 2015, doi: 10.1038/micronano.2015.2.

Kevin A. White (Member, IEEE) received the Ph.D. degree in electrical engineering from the University of Central Florida (UCF), Orlando, FL, USA, in 2021.

He is currently a Research Associate with the Dr. Brian N. Kim's Bioelectronics and Neuroengineering Laboratory, The University of Texas at Dallas, Richardson, TX, USA. His research interests include circuit design, digital signal processing, post-CMOS processing, microelectrode fabrication, and brain–machine interfacing.

Mahdieh Darroudi received the Ph.D. degree in organic chemistry from the University of Mazandaran, Babolsar, Iran, in 2017.

She joined the University of Central Florida, Orlando, FL, USA, as a Postdoctoral Researcher. She is a Research Associate with the Dr. Brian Kim's Laboratory, The University of Texas at Dallas, Richardson, TX, USA, focusing on fabricating nano biosensors for neurotransmitter measurement. Her primary research interests lie in the development and application of advanced nanomaterials for biosensing technologies. During her doctoral studies and subsequent research positions, she has contributed to organic chemistry and nanotechnology, demonstrating a keen interest in the interface of chemistry and bioengineering.

Jinwoo Park received the Ph.D. degree in analytical chemistry from Dr. Greg Swain, Michigan State University, East Lansing, MI, USA, and the Ph.D. degree in chemistry/neuroscience from the University of North Carolina, Chapel Hill, NC, USA, in 2006, under the supervision of Dr. Mark Wightman.

He is currently an Associate Professor with Biotechnical/Clinical Laboratory Sciences, Buffalo Jacob School of Medicine and Biomedical Sciences, State University of New York (SUNY), Buffalo, NY, USA. His research focuses on neurochemical sensor development, understanding catecholamine neuronal functions in the brain, and the dysfunction of catecholamine systems in disease states.

Brian N. Kim (Senior Member, IEEE) received the Ph.D. degree in biophysics from Cornell University, Ithaca, NY, USA, in 2013.

From 2013 to 2014, he was a Postdoctoral Fellow of Bioengineering with the University of California, Berkeley, CA, USA. From 2014 to 2015, he was a Senior Electrical Engineer with Stratos Genomics (now, Roche Diagnostics Sequencing), Seattle, WA, USA. He is currently an Associate Professor of Bioengineering with the University of Texas at Dallas, Richardson, TX, USA. His research interests include neural engineering, single-cell electrophysiology, and brain–machine interface.